INFLUENCE OF VARIOUS FACTORS ON THE PREDIC TIONS FURNISHED BY CFD IN CROSS-VENTILATION SIMULATIONS

G.O. Freskos

Centre for Renewable Energy Sources, Athens, GREECE

ABSTRACT

The results of various numerical simulations of wind induced flows through large openings in a room are presented. The study is parametric on the sizes and relative positions of the openings and the wind direction. Various grid densities have been used. Grid independency for the presented results is demonstrated. Validation of the numerical approach is performed using measurements on a test cell with a single opening. The influence of the inflow wind profile is studied. It is shown that different flow patterns are induced within the dwelling when different profiles are assumed. In a two-zone room the main flow is deviated, due to the presence of the partition. The partition increases the obstruction of the flow entering the room. On the other hand better distribution of the flow within the room is obtained.

KEYWORDS

Air flow pattern, CFD, Cross ventilation, Numerical methods, Ventilation efficiency

INTRODUCTION

Natural ventilation is widely used in warm climates to improve comfort. Its effects depend upon the temperature and the speed of the incoming wind flow. More particularly, the air flow speed and the flow patterns induced within the enclosure are the most decisive factors in relieving the hot sensation, since air temperature is difficult to control in such configurations. Furthermore, if proper care is taken regarding the positioning and sizing of the openings, it can be possible to obtain a desired air flow distribution. The efficacy of the configuration will depend upon the wind characteristics of the region (direction and speed).

Computational Fluid Dynamics (CFD) has emerged in recent years as a strong alternative to wind tunnel testing for predicting wind effects in and around buildings (Walker 1992). Compared to wind tunnel simulations, CFD may provide more detailed and comprehensive information concerning the flow structure.

Relating to ventilation problems, a number of works appeared, using mainly commercial packages. The flow around buildings has been studied in (Delaunay et al. 1995), (Riley et al. 1996), (Tsutsumi et al. 1996). Other authors worked on predicting the flow patterns within rooms, for cases of forced or free convection (Awbi 1989), (Wang et al. 1991), (Haghighat et al. 1992).

In this work, we present the results of CFD simulations, of wind induced flows through large openings in a room. The study is parametric on the sizes and relative positions of the openings and the wind direction.

The PHOENICS code has been used in several occasions to compute flow fields, for a diversity of flow driving mechanisms (as deduced by the boundary conditions). Its characteristics (at least those that have been used in the present work) are summarised in the following section.

NUMERICS / MODELS

The general equations describing the flow are those expressing the conservation of mass and momentum for an incompressible fluid (the energy equation is not solved, since the flow is considered isothermal). The set of partial differential equations (PDEs) expressing these laws, for steady flows, are the following (in average form to account for turbulent effects):

$$\frac{\partial U_i}{\partial x_i} = 0 \qquad (1)$$

$$U_j \frac{\partial U_i}{\partial x_j} = -\frac{1}{\rho} \frac{\partial P}{\partial x_i} + \frac{\partial}{\partial x_j} \left(\nu \left(\frac{\partial U_i}{\partial x_j} + \frac{\partial U_j}{\partial x_i} \right) - \overline{u_i u_j} \right) \quad (2)$$

where, ρ, U_i and P are the density, mean velocity components and pressure, respectively. ν is the laminar viscosity and $\overline{u_i u_j}$ are the momentum turbulent fluxes.

In order to solve the above equations, pressure correction methods are widely used. PHOENICS is based on such an algorithm, the SIMPLE method (Phoenics lectures 1995): Given an initial pressure field, the momentum equations furnish the velocities. Subsequently, the continuity equation provides errors in each grid cell. A pressure-correction equation is then constructed, which gives corrections for both the pressure and velocity fields. The sequence is repeated with the new pressure distribution.

The SIMPLEST variation (Markatos & Pericleous 1984), which is actually used by PHOENICS, ensures more rapid convergence. The convection terms of the governing equations are discretized using the hybrid-differencing scheme.

The finite volume form of the equations are solved using a strongly implicit procedure in a plane (Thomas tridiagonal algorithm or SIP) and sweeping in the third direction. Alternatively, the Point by Point (Jacobi) method can be used, usually for the velocity and especially when viscosity is unimportant. Whole field solution can be specified for all scalar variables. (Whittle 1986). This can be especially beneficial for the pressure correction equation, since effects of flow boundary conditions and blockages are then rapidly transmitted throughout the domain.

The $\overline{u_i u_j}$ terms of eq.(2) represent additional unknowns, which should be either modelled, or solved for, through the introduction of additional equations. The most widely used approach is to link the turbulent fluxes to the mean velocity gradient, through the introduction of the turbulent viscosity (ν_t):

$$\overline{u_i u_j} = -\nu_t \left(\frac{\partial U_i}{\partial x_j} + \frac{\partial U_j}{\partial x_i} \right) + \frac{2}{3} k \delta_{ij} \quad (3)$$

$$\nu_t = C_\mu \frac{k^2}{\varepsilon} \quad (4)$$

In the two-equation turbulence models, the turbulent viscosity is related to two supplementary quantities, which are in turn computed by solving corresponding transport equations. In the case of the k-ε model, these equations are the following:

$$U_j \frac{\partial k}{\partial x_j} = \frac{\partial}{\partial x_j} \left(\left(\nu + \frac{\nu_t}{\sigma_k} \right) \frac{\partial k}{\partial x_j} \right) + P_k - \varepsilon \quad (5)$$

$$U_j \frac{\partial \varepsilon}{\partial x_j} = \frac{\partial}{\partial x_j} \left(\left(\nu + \frac{\nu_t}{\sigma_\varepsilon} \right) \frac{\partial \varepsilon}{\partial x_j} \right) + C_1 P_k \frac{\varepsilon}{k} - C_2 \frac{\varepsilon^2}{k} \quad (6)$$

$$P_k = \nu_t \frac{\partial U_i}{\partial x_j} \left(\frac{\partial U_i}{\partial x_j} + \frac{\partial U_j}{\partial x_i} \right) \quad (7)$$

In equations (4)-(7) δ_{ij} is the Kronecker symbol and C_μ, C_1, C_2, σ_k and σ_ε are constants of the model. Their values are the standard ones (Launder & Spalding 1974).

If no "low-Reynolds number" corrections are introduced in (4)-(6), wall functions should be used to properly treat solid wall boundaries. In the present computations the k-ε model of Launder & Spalding (Launder & Spalding 1974) is used. Wall functions for rough wall flow are used on the ground boundary and on the faces of the room. In PHOENICS the effect of roughness is taken into account by modifying a parameter in the logarithmic law, according to the empirical laws proposed by (Jayatilleke 1969) for "sand-grain" roughness.

The grid is staggered, i.e. the scalar quantities are computed in cell centres, whereas velocities are calculated on cell interfaces.

BOUNDARY CONDITIONS

The atmospheric boundary layer is known to be extremely turbulent. Turbulence intensities of the order of 20-30% are not rare in atmospheric flows. The thickness of the atmospheric boundary layer extends over

(WxH = 1.6x2.2) and a window (WxH = 1.3x2.2) were placed at the middle of the corresponding wall (if not specified). A cartesian grid of 59, 50 and 37 in the I, J, K directions respectively (I and K are the main flow and vertical directions, respectively).

The velocity profile was adimensionalized by dividing it with the wind velocity V_{REF} at Z=3m (the room height).

Three wind directions have been considered: 0°, 22.5° and 45°, relative to the normal on building's windward wall.

The results for the above configurations and parametrical runs are presented in the following paragraphs. Additionally, we present in (i) below, results obtained on a configuration, for which measured velocity profiles are available.

(i) **The PASSYS test cell:** Experimental results were published from the flow in a single-sided ventilated room, the so-called PASSYS test cell (Dascalaki et al. 1996). The opening dimensions were HxW = 2x1.01 [m], whereas the room area was 8.6m² (L=2.4m, H=3.29m). A series of experiments have been conducted, with approximately isothermal conditions. Although no clear information on wind direction and profile is provided (due to lack of control), we have tried to simulate the experimental set-ups and compare the numerical results with the available measurements. The mean wind speeds at 10m for the simulated experiments were 3.3m/s, 2.5m/s and 3.6m/s. For the various simulations suburban velocity profiles have been imposed at the inflow boundary.

Measurements have been reported at the middle of the opening. They concerned mean air velocities, measured using hot-wires. The published data, along with the numerical predictions are given in figs. 1-3. The vertical segments in these figures represent standard deviation of the measurements. Uncertainty is quite elevated. If the above factors are taken into account, the accordance between experiment and predictions may be judged satisfactory, especially in the lower part of the opening. The dis-

crepancies appearing in the upper part may be attributed to the fact that the door's width has been neglected in the computations.
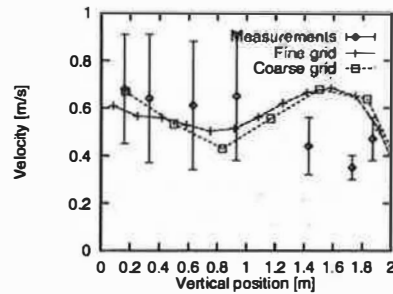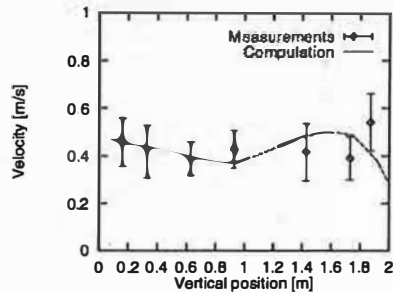

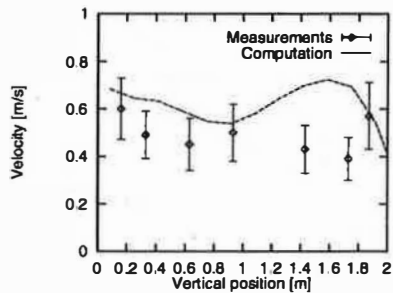Figure 1. PASSYS cell - Vref=3.3m/s

Figure 2. PASSYS cell - Vref=2.5m/s

Figure 3. PASSYS cell - Vref=3.6m/s

On fig.1, predictions using two different grids are presented. The coarse grid has 26, 25 and 19 points in the I,J,K directions respectively. In the finer grid the double number of points are used along each direction. Comparison of the two computed curves, suggests that there is no substantial differences between them. Nevertheless, we have used in subsequent computations, the finer grid to better capture patterns appearing in the flow.

486

several hundred meters. This means that, as opposed to most flows which are usually encountered in Aerodynamics, the computation domain when studying the flows around buildings is entirely contained within the boundary layer.

Of great importance for atmospheric flows, is the roughness of the region, over which the flow is considered. This is mirrored in the well-known Log Law which represents the velocity profile:

$$\frac{U}{U_*} = \frac{1}{\kappa} \ln\left(\frac{Z-d}{Z_0}\right) \qquad (8)$$

where Z_0 is the equivalent sand roughness height and d is the displacement thickness. When using this expression in a numerical modelling, care should be taken for the first computation node, adjacent to the wall, to be at a distance from the latter superior to both Z_0 and d. Typical values for the sand roughness height are 0.03m for flat terrain, 0.3m for suburban and 3.m for urban boundary layers (ASHRAE 1989). U^* is the friction velocity $(=\sqrt{(\tau_w/\rho)})$, and κ is the Von Karman constant (=0.40).

A simpler expression is given by the power law, which relates the velocities in two different heights as follows:

$$\frac{U}{U_0} = \left(\frac{Z}{Z_0}\right)^a \qquad (9)$$

where U_0 is the wind speed at a reference height Z_0. Typical values for the exponent α are 0.15, 0.28 and 0.40 for flat terrain, suburban and urban boundary layers, respectively.

Measurements of the atmospheric turbulence, tend to certify that the ratios of the standard deviations of all three fluctuation velocity components to the friction velocity remain constant in the boundary layer. The following values are registered, according to (Panofsky & Dutton 1983) (x_1 is the mean wind direction):

$$\frac{\sigma_{u_i}}{U_*} = (2.39 \pm 0.03, 1.92 \pm 0.05, 1.25 \pm 0.05) \qquad (10)$$

or,

$$\sigma_{u_1} : \sigma_{u_2} : \sigma_{u_3} \approx 1 : 0.8 : 0.5 \qquad (10b)$$

where, $\sigma_{u_i}^2 = \overline{u_i^2}$ and $k = \frac{1}{2}\sigma_{u_i}^2$.

The turbulence intensity, is defined as

$$I_{u_1} = \frac{\sigma_{u_1}}{U_1} \qquad (11)$$

If isotropic turbulence is assumed, or if the u_2, u_3 velocity fluctuation components are neglected, the following relations are obtained, respectively:

$$k = \frac{3}{2}\left(I_{u_1} U_1\right)^2, \text{ or } k = \frac{1}{2}\left(I_{u_1} U_1\right)^2 \qquad (12)$$

The turbulent dissipation profile is usually defined through some length scale or constant ratio of turbulent to laminar viscosity assumption. In the present work the second approach has been followed.

At inflow boundaries the mass flow rate is prescribed by imposing a boundary layer, following either equations (8) or (9), along with the deduced turbulent energy (eq. (12)) and dissipation profiles. The outflow section is a constant pressure boundary.

SIMULATIONS & RESULTS

A grid around an orthogonal room has been used. It should be pointed out, that the outdoor and indoor flows have completely different scales. This may, in some extent, be taken into account, by using different grid densities in the two regions. The grid density is increased close to wall boundaries by using geometric progressions.

The dimensions of the room were LxWxH = 6x4x3 [m]. The dimensions of the discretization domain were LxWxH = 18.6x8x6 [m]. Position of openings on windward, leeward and lateral walls have been tested. As typical openings a door

the results of figs. 7, follow the exponential law as proposed for a suburban boundary layer (α=0.28). We have also investigated the influence of the exponent (i.e. the nature of the boundary layer), on the predicted flow field. More precisely, the value of the exponent α has been set to 0.40 (urban boundary layer). At this point, it should be noted that we do not expect this value to be of relevance to cross-ventilation problems, at least for the configurations discussed here, since urban boundary layers are characterised by roughness sizes of the order of meters and therefore they should be used for much higher buildings. We have nevertheless proceeded to the investigation of this case, in order to examine the influence of this important parameter to the predicted flow field.
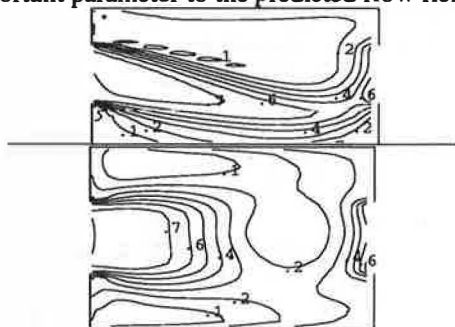
Figure 7. As in Fig.6 with Urban Inflow Vprofile

Comparisons of figs.7 to the corresponding ones (figs. 6) for the suburban profile, show that when the urban profile is used the downwash flow is much more pronounced. Furthermore, the mean velocity at z=1.5m is considerably reduced. This is also connected to a lower ach rate compared to the one obtained for the suburban case. The above behaviour should be attributed to the more pronounced shear of the urban profile, facilitating the mixing phenomenon downstream of the windward opening.

(v) **Front and Lateral openings:** The second opening is now placed on one of the lateral walls. The openings are of the same size and located at the same vertical position. The flow is deviated towards the outflow opening (figs. 8). The maximum velocities attained within the enclosure are inferior to the ones predicted for the opposite windows

configuration. On the contrary, higher velocities are predicted in the corner regions and the extent of the stagnation zones is reduced. The vortex developing in the leeward corner of the enclosure may considerably improve the ventilation of this region.
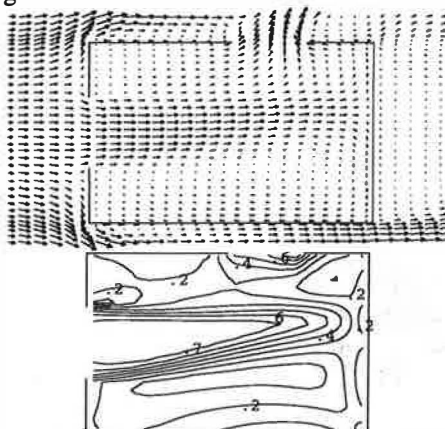

Figure 8. Velocity vectors & contours at z=1.485m

(vi) **Wind incidence:** We have investigated the influence of the flow incidence on the flow patterns induced within the enclosure, and consequently on the ventilation efficiency. Two values of the flow incidence have been used; namely 22.5° & 45° with respect to the normal to the upstream wall.
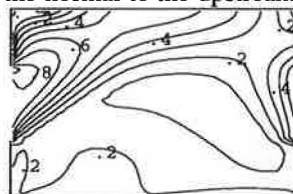

Figure 9. Opposite Windows / 22.5°Incidence: Abs. Vel. Contour lines at z=1.485m

In the first case, the region of high velocities is restricted to a small zone very close to the inflow window. The absolute velocity values are more moderate compared to the 0° case and more homogeneously distributed over the entire space of the enclosure. Furthermore, an extensive mixing is taking place (fig.9), improving considerably the ventilation characteristics of the configuration. The 45° incidence (figs. 11-12) presents a region of very high velocity values at the inflow window. The bulk of the flow takes place very close to the upper wall of
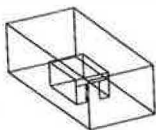
(ii) Single opening: The penetration length, predicted according to fig. 4, can be estimated to more than 50% of the room length -at least close to the ground- where velo ies of more than 10% of the reference velocity can be measured. Two vortices of opposite direction are readily perceivable on the opening mid-span plane. A strong one is located at the opening, whereas a much weaker and extended one can be perceived versus the opposite to the opening wall.
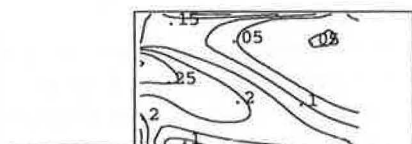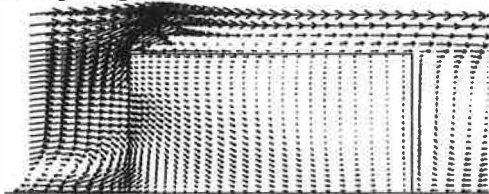

Figure 4. Vel. vectors & contours at door midspan
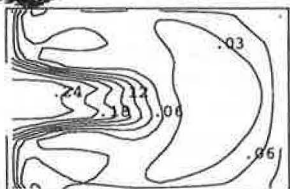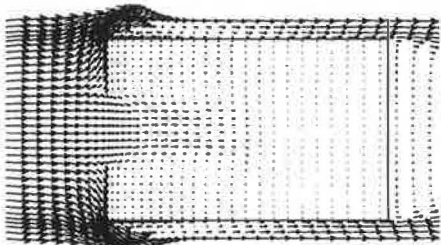
Figure 5. Vel. vectors & contours at z=1.485m

On fig. 5, presenting velocity vectors and contour lines at $z\approx1.5$m, the penetration length is much more reduced (~40% of the room length). This is due to the downwash nature of the flow. The "vena contrata" behaviour of the incoming jet flow is clearly illustrated. The absolute velocity values in the larger part of the room remain very weak (< $0.06*V_{REF}$). Nevertheless, the obtained ach rate for the specific configuration can be in acceptable levels (depending on freestream velocity), although some extended recirculation zones appear, at the opposite to the opening region and at the corners behind the front walls.
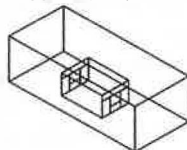
(iii) Opposite windows: The field induced for this configuration is characterised by the downwash flow within the room (fig. 6a). This should be attributed to the shear connected with the boundary layer profile impinging on the upstream wall. The downwash flow is disturbed towards the outflow window, where the suction region behind the room provokes a local acceleration and directs the flow upwards to the outlet.
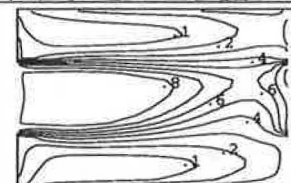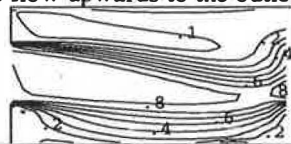

Figure 6. Vel. Contours at Midspan & z=1.485m

Extended regions of elevated velocity are predicted (see fig. 6b). Values as high as 80-90% of the reference velocity are developing within the room. It should be mentioned that these high values are constrained in "tube" between the two openings. The lateral areas of the enclosure are covered by lower velocities (10-20% of V_{REF}). The computed ach rate for this case is superior to the one (approximate) induced if the ASHRAE formulae are used (ASHRAE Fundamentals 1989).

(iv) The inflow velocity profile: As discussed in a previous paragraph, the velocity profile imposed at the upstream boundary of the domain, obeys the exponential law, which is an easier to use approximation to the log-law. The profiles in all but

487

fig.11, whereas the remaining main part of the room is subject to low values of the absolute velocity. Nevertheless, fig.12a dictates an important circulation from the bottom to the upper limits of the enclosure (x measured from upstream wall). High velocities are restricted to the left wall of fig.12b.
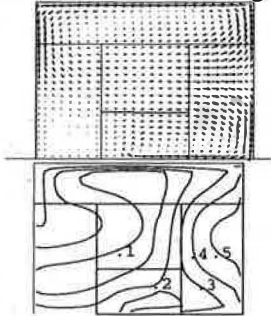

Figure 10. Opposite Windows / 22.5°Incidence: Abs. Vvec & Contour lines at x=2.1m
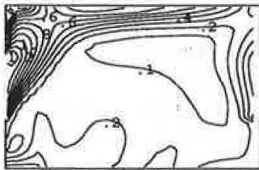

Figure 11. Opposite Windows / 45.0°Incidence: Abs. Vel. Contour lines at z=1.485m
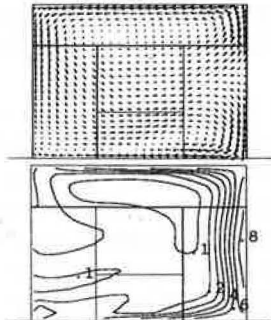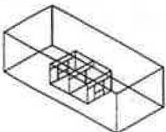

Figure 12. Opposite Windows / 45.0°Incidence: Abs. Vel. Vectors & Contours at x=2.1m

If some general remarks are to be drawn, the 22.5° configuration presents the best flow patterns, from the three configurations studied. This is with regard to the most homogeneous velocity distribution within the enclosure.

(vii) Two-zone enclosure: A partition with a door opening has been added to the dwelling. The partition wall has been placed at 3m from the upstream wall (the length of the dwelling is 6m). The dimensions of the door are WxH = 1.6x2.2 [m]. The main flow is deviated, due to the presence of the partition. The high speed flow is then concentrated near to the wall adjacent to the partition door, before it reaches the outflow opening. The partition increases the obstruction of the flow caused by the room. This can be verified by the much lower values of the maximum velocity obtained for this case, as compared to those predicted for the opposite windows configuration (fig.13b). Consequently the computed ach rate is expected to be lower.
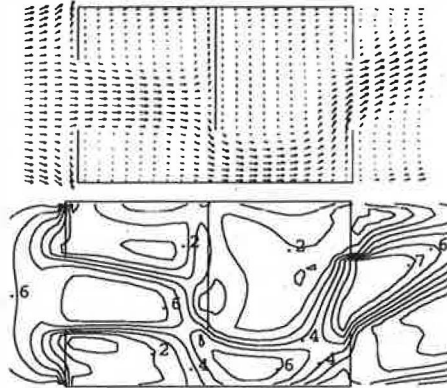

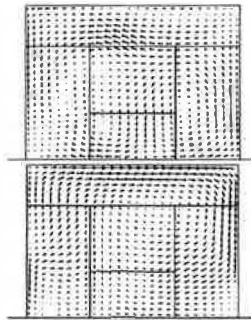**Figure 13. Vel. Vectors & Contours z=1.485m**

Figure 14. Vel. Vectors at x=1.5m & 4.48m

Vortices appearing in the two zones promote the homogeneity of the flow field within the enclosure. A minimum value of 20% of the reference velocity are computed even at 'difficult' regions. The velocity vectors presented at positions upstream and downstream of the partition (figs.14) demonstrate the complicated structure of the flow field and show the movement of the

489

vortices (y-z plane) from the first zone (vortex located close to the bottom left corner) to the second zone (main vortex located in the upper part of the zone). This suggests an important mixing of the flow, covering the greatest part of the two-zone enclosure.

CONCLUSIONS

The study presented in the current work has tried to encompass various factors of elevated significance for the predictions furnished by CFD methods in cross-ventilation problems. Furthermore, we have also tried to investigate numerically the effect of opening positions in ventilation efficiency. Comparison with an experimentally investigated case has shown that standard CFD can reproduce measurements, provided that care has been taken to be in accordance with the boundary conditions and the geometry of the configuration.

One of these conditions that have proved to play an extremely important role, is the boundary layer profile imposed at the entrance of the computational domain. Thoroughly different flow patterns are deduced if different exponents (or equivalently surface roughness) are used.

The ventilation efficiency may be improved if a number of points are properly taken into account:

- orientation of the dwelling with respect to the locally prevailing wind directions. In general, a perpendicular to the windward opening wind will not provide the optimal ventilation efficiency (regarding at least the flow distribution within the room),
- proper positioning of the openings (not facing each other) may promote mixing of the flow within the space,
- interior partitions have the same effect, although they may increase flow obstruction.

REFERENCES

ASHRAE (1989) *Fundamentals Handbook.*

Awbi, H.B. (1989) Application of CFD in room ventilation, *Building & Environment*, 24(1), 73—84.

Delaunay, D., Lakehal, D. and Pierrat, D. (1995) Numerical approach for wind load predictions on buildings and structures, *Journal of Wind Engineering. and Aerodynamics*, 57, 307-321.

Haghighat, F., Jiang, Z., Wang, J.C.Y. and Allard, F. (1992) Air Movement in buildings using CFD, *ASME Transactions*, 114, 84-92.

Jayatillike, C.L.V. (1969) The influence of the Prandtl number and surface roughness on the resistance of the sublayer to momentum and heat transfer, *Prog. in Heat & Mass Transfer*, 1.

Launder, B.E. and Spalding, D.B. (1974) The numerical computation of turbulent flow, *Comp. Meth. in Appl. Mech. & Engng.*, 3, 269.

Markatos, N.C. and Pericleous, K.A. (1984) Laminar and turbulent convection in an enclosed cavity, *Int. Journal of Heat and Mass Transfer*, 27-5.

Panofsky and Dutton (1983) *Atmospheric turbulence*.

PHOENICS on line help (1995) CHAM.

Riley, W.J., Gadgil A.J. and Nazaroff, W.W. (1996) Wind-induced ground-surface pressures around a single family house, *Journal of Wind Engineering and Aerodynamics*, 61, 153-167.

Tsutsumi, J., Katayama, T., Ishii, A., He, P. and Hayashi, T. (1996) Investigation and numerical simulation of the wind effects on thermal comfort in a house, *Journal of Wind Engng. and Aerodynamics*, 60, 267-280.

Wang, J.C.Y., Jiang, Z. and Haghighat, F. (1991) Influence of air infiltration on airflow in a ventilated isothermal two-zone enclosure, *Energy & Buildings*, 17, 43-54.

Walker, G.R. (1992) Wind engineering beyond the boundary layer wind tunnel, *Journal of Wind Engineering and Aerodynamics*, 41-44, 93-104, (1992).

Whittle, G.E. (1986) Computation of air movement and convective heat transfer within buildings, *International Journal of Ambient Energy*, 7(3), 151-164.